1-s2.0-S1526612520307039-main_Jurnal_Bowo_Q1.pdf

by

Strength and fatigue crack growth behaviours of metal inert gas AA5083-H116 welded joints under in-process vibrational treatment

M.N. Ilman [a,*], R.A. Sriwijaya [a], M.R. Muslih [b], N.A. Triwibowo [c], Sehono [a]

[a] Department of Mechanical and Industrial Engineering, Universitas Gadjah Mada (UGM), Yogyakarta, Indonesia
[b] National Nuclear Energy Agency of Indonesia (BATAN), Serpong, Banten, Indonesia
[c] Sekolah Tinggi Teknologi Adisutjipto (STTA), Yogyakarta, Indonesia

ARTICLE INFO

ABSTRACT

Strength and fatigue properties are important design considerations for many aluminium welded structures which are operated under cyclic loadings such as ships, railway vehicles and car bodies. Over the years, various weld treatments have been developed to improve the quality of weld joints through modification of microstructure and residual stress. In the present study, in-process vibrational treatment has been applied to metal inert gas (MIG) welding of 5083-H116 aluminium alloy plates at various frequencies of 100, 300 and 500 Hz in effort to enhance strength and fatigue crack growth resistance of the weld joints. Experimental works including microstructure observation, microhardness and tensile tests, residual stress measurements and fatigue crack growth tests were performed. Results showed that in-process vibrational treatment obviously increased the ultimate tensile strength of the weld joints with the best frequency was achieved at 300 Hz. It was found that the strength of the weld at this condition was increased around 51.3 % higher than the weld in as welded condition owing to grain refinement and increasing amount of equiaxed dendritic microstructure in the weld metal region. These fine grained equiaxed dendritic structures combined with compressive residual stress induced by vibrational treatment could improve fatigue crack growth performance of the welds.

Introduction

The application of mechanical vibration in fusion welding processes has been the subject of numerous research works since the 20th century with the main objective of improving mechanical properties of certain regions of weld joints such as fusion zone (weld metal) and heat affected zone (HAZ). This vibrational treatment can be conducted either during welding known as vibration assisted welding (VAW) or after welding named vibration stress relief (VSR) [1]. The former can be categorised as in-process treatment and it is intended for improving weld microstructure through modification of solidification and stress relieving process whereas the latter is designed for stress relieving only. The advantages of vibrational technique over thermal treatments are that the vibrational treatment is convenience in operation, it requires shorter manufacturing process, it produces less pollution and more importantly, less investment is required [2]. However, the application of this technique is restricted to soft materials and thin sheets due to limited available power of ultrasonic transducers or vibration exciters [3].

The mechanisms in which mechanical vibration to influence weld solidification and hence the resultant microstructure have been studied extensively by numerous researchers. Cui et al. [4] have shown that ultrasonic vibration applied during welding generates acoustically induced cavitation and streaming resulting in a complete mixing of melted filler metal and base metal. As a consequence, unmixed zone which generally exists in conventional weld metal is eliminated. Other researchers [5,6] have suggested that the introduction of ultrasonic vibration leads to modification of microstructure in the weld metal from columnar to equiaxed grains whereas the degree of microstructural changes in the weld metal and HAZ is dependent on a wave phase [7]. To date, it is well known that the beneficial effect of vibrational treatment applied during welding on weld mechanical properties is associated with grain refinement produced by mechanical vibration through the fragmentation of dendrites and grain detachment which promote heterogeneous nucleation during solidification [8–10]. In addition, the grain refining of welds can increase resistance to hot cracking, reduce weld porosity and segregation [6,11].

The use of vibration for grain refinement has long been known in casting process and according to Campbell [12], the effectiveness of

---

grain refinement is controlled by excitation frequency and amplitude, typically in the range of 1 to 10^5 Hz and 0.1 to 10^4 µm respectively. Since solidification in casting is not too much different to welding process so that in-process vibrational treatment can be performed using a wide range of frequencies as well, either below 20 kHz (subsonic/sonic vibrations) or higher than 20 kHz (ultrasonic vibration). While vibration assisted welding processes are conducted massively using ultrasonic vibration, the use of low frequency vibration for in-process vibrational treatment is proved to be effective as well. Tewari [13] has shown that low frequency vibration with the frequency and amplitude in the range of 0–400 Hz and 0–40 µm respectively can effectively refine dendrites during weld solidification. Recently, Tamasgavabari et al. [14] have reported that vibration assisted MIG welding with a frequency below the resonance range, typically 50 Hz increases tensile strength of the MIG 5083-H321 aluminium alloy weld joint due to grain refinement.

During the past few years, mechanical properties of vibration assisted weld joints have been extensively studied including tensile stress [15–17] and impact toughness [13,18]. The general conclusion obtained from these works is that the grain refinement resulted from vibrational treatment is responsible for improved strength and toughness of the welds. However, confusion still exists regarding the hardness of the welds vibrated during welding. Some researchers [19–21] have shown that vibrational treatment enhances the hardness of the weld joints due to work hardening. According to them, this hardening is caused by numerous split dislocations generated during vibration of the hot weld metal whilst others [18,22] show contradicting results. These different results are probably due to the fact that there are too many parameters involved during welding process.

In aluminium or steel welded structures which are designed to operate under dynamic loads, fatigue property of weld joints is extremely important and it is strongly influenced by residual stress in the weld joints [23,24]. In general, residual stress can be reduced using post weld heat treatment, i.e. stress relief annealing, commonly performed at temperature in the range of 450–700 °C for mild and low alloy steels [25]. However, in certain cases such as welding of S355 steel, the heat treatment has been reported to reduce fatigue lifetime of the welds due to microstructural changes, from martensite-bainite microstructure to a mixture of bainite and sorbite [26]. Based on the fatigue crack path analysis, the authors suggest that the performed heat treatment procedure can modify the residual stress state in the crack path resulting in high tensile residual stress near the crack paths. Apart from residual stress, the fatigue behaviour of the weld is also affected by plate thickness and fillet weld end geometry despite their effects are relatively low [27].

The use of mechanical vibration for stress relieving (VSR) to improve weld fatigue performance has long been the subject of extensive studies. However, from the view point of engineering implementation, VSR is a time-consuming process since it requires additional work after welding and therefore, vibration assisted welding (VAW) or in-process vibrational treatment may be desirable. Recent investigations [28,29] have shown that the introduction of vibration during welding improves fatigue life of weld joints due to fine grained structure present in the weld metal region and reduced residual stress. Despite fatigue studies on vibration assisted weld joints have been conducted extensively, however the majority of them are focused on fatigue life enhancement of the weld joints and unfortunately, there have been few studies devoted to their fatigue crack growth behaviour. Therefore, this becomes subject of the present study.

Experimental procedure

The materials used in this investigation were 5083-H116 aluminium alloy plates (3 mm × 100 mm × 300 mm) and ER5346 filler metal with their chemical compositions are given in Table 1. The welding parameters used in this investigation are given in Table 2. A metal inert gas (MIG) welding machine was designed automatically as shown in Fig. 1 to improve consistency. A vibration exciter (laboratory shaker) was located underneath the weld region with its position in the middle part of the welded plate length to generate vibration assisted welding (VAW). The plates were gently clamped at both plate ends hence forming cantilevered plates. Three thermocouples, namely Tc1, Tc2 and Tc3 were placed at the distances of 10, 20 and 30 mm respectively from the weld centreline to monitor temperatures during welding.

To determine the frequencies used in this work, the plates were first vibrated in a vertical direction (or perpendicular to the plates) at various frequencies prior to welding and each response displacement amplitude, a_o at a predetermined frequency, f was measured using a vibration meter hence resulting in a plot of a_o vs. f as shown in Fig. 2. If this transverse vibration of the plates is simplified and it is assumed to be a system with one degree of freedom in steady state force condition with no damping, then the curve in Fig. 2 can be approached by magnification factor, β which amplifies displacement amplitude as frequency moves towards the natural frequency, f_n as follow [30]:

$$\beta = \left| \frac{1}{1 - (\omega/\omega_n)^2} \right| \tag{1}$$

where ω is angular speed which is defined as $\omega = 2\pi f$ whereas ω_n is natural angular frequency. From Fig. 2, the value of natural frequency, f_n was estimated to be 45 Hz. Of note is that the use of frequency near f_n of the system should be avoided since it can cause violent agitation in a weld pool due to a sharp increase in displacement amplitude according to Eq. (1). Therefore, the minimum frequency used in this investigation was set at 100 Hz in order to prevent violent agitation, above which the displacement amplitude decreases asymptotically towards zero. Based on these results, the frequencies of 100, 300 and 500 Hz were selected in this study giving response amplitudes of 81, 5 and 5 µm respectively.

After completion of welding, the locations of test specimens were determined as shown in Fig. 3a followed by sectioning. The details of centre-cracked tension (CCT) specimen are shown in Fig. 3b. Samples for microstructural observation were sliced in the direction perpendicular to the weld length. The samples were prepared according to a standard metallographic technique using the etchant of Keller reagent. Fig. 4 shows typical microstructures of AA5083-H116 base metal taken from longitudinal (L), short transverse (ST) and long transverse (LT) directions observed under optical microscopy. Such microstructures are typical of a wrought product marked by grain elongation along the

Table 2
Materials and welding parameters.

Wire diameter	0.8 mm
Wire speed	8 m/min.
Shielding gas	Argon (Ar)
Gas flow	15 L/min.
Voltage	20 V
Current	130 A
Welding speed	10 mm/s

Table 1
The chemistries of 5083-H116 plates and ER 5356 filler metal (wt.%).

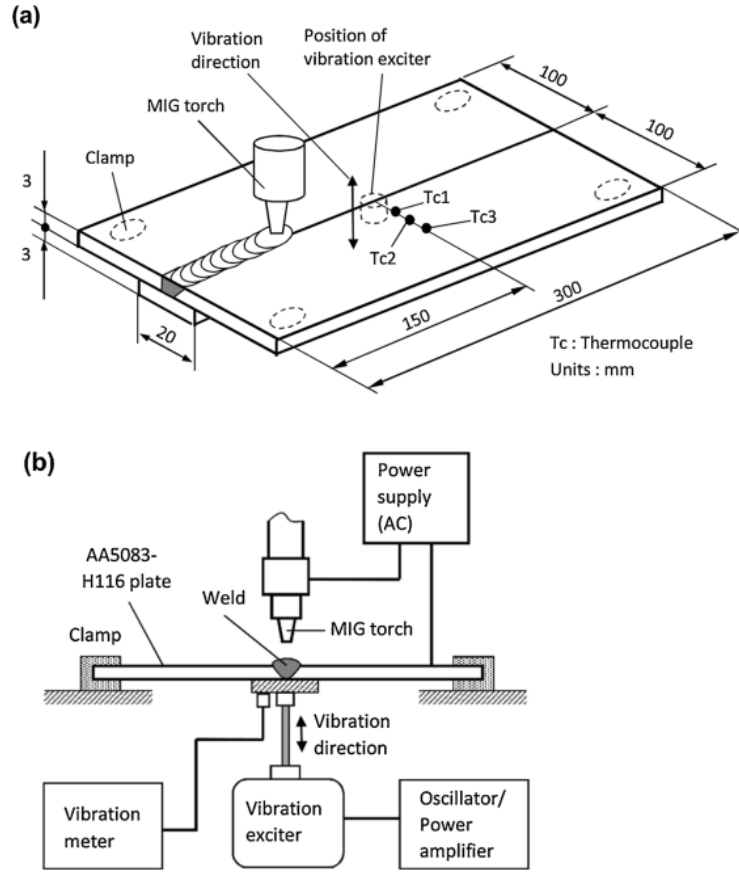| Material	Mg	Mn	Si	Fe	Cr	Cu	Zn	Ti	Al
AA 5083-H116	4.5	0.65	0.26	0.22	0.09	0.09	0.06	0.03	Bal.
ER 5356 filler	4.5–5.5	0.05–0.20	0.25	0.40	0.05–0.20	0.10	0.10	0.06–0.20	Bal.

(a)

(b)

Fig. 1. (a) An experimental set-up for welding under in-process vibrational treatment; (b) a schematic diagram of arrangement for in-process vibrational treatment.
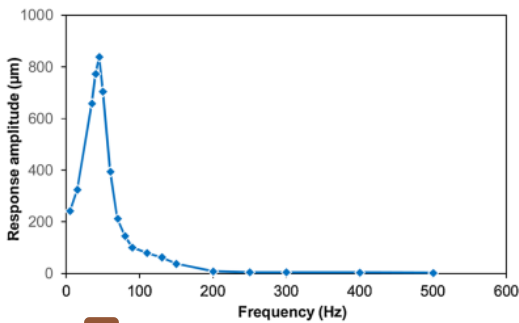

Fig. 2. Plot of response amplitude as a function of frequency.

rolling direction. Subsequently, Vickers microhardness measurements were conducted across the weld joints using a load of 100 grf. Tensile tests were carried out using transverse weld specimens according to ASTM E8M [31]. Each welding treatment was tensile tested in triplicate to ensure reproducibility. No sectioning process was required for residual stress measurements.

The fatigue crack growth (FCG) tests were conducted using a servo-hydraulic machine. Centre-cracked tension (CCT) specimens were prepared according to ASTM E647 [32] with the position of the weld perpendicular to the applied stress as shown in Fig. 3b. For each weld specimen, the initial crack was machined using electrodischarge

machine (EDM) in the weld region with the crack direction parallel to the weldline whereas the initial crack in CCT specimens for 5083-H116 base metal was made in L–T orientation. A sinusoidal load having a constant load amplitude with a maximum load, P_{max} of 6000 N was applied during FCG tests. In order to identify effect of residual stress on fatigue crack growth rate behaviour, a low stress ratio, R typically of 0.1 was used at the frequency of 11 Hz. The fatigue crack length measurements as a function of cycles were conducted using a traveling microscope for every crack length increment of 0.1 mm. The fatigue crack growth rates were then determined by incremental polynomial method. Subsequently, fractographic studies were conducted using scanning electron microscopy (SEM). Of note is that this FCG study was performed using one test only for the base metal and each weld joint under different treatments. Despite the number of specimens was not sufficient statistically but the inherent experimental scatter in the experimental results were probably minimised due to the use of welding automation which helped to provide consistency. Nevertheless, more experiments would be required for future work.

Weld residual stresses were assessed using neutron diffraction technique at the National Nuclear Energy Agency of Indonesia (BATAN). The residual stress measurements were taken along the transverse distance from the weld centreline the middle part of the welded plate length as shown in Fig. 3a. The neutron beam with a wave length of 1.833 Å was selected and the measurements were conducted using the Al (311) reflection at the detector angle, 2θ of around 96.5°. To obtain acceptable neutron count rates, a gauge volume size of 8 mm^3 ($2 \times 2 \times 2$ mm^3) was used because this gauge volume was sufficiently large in comparison with the grain size hence allowing a statistically representative number
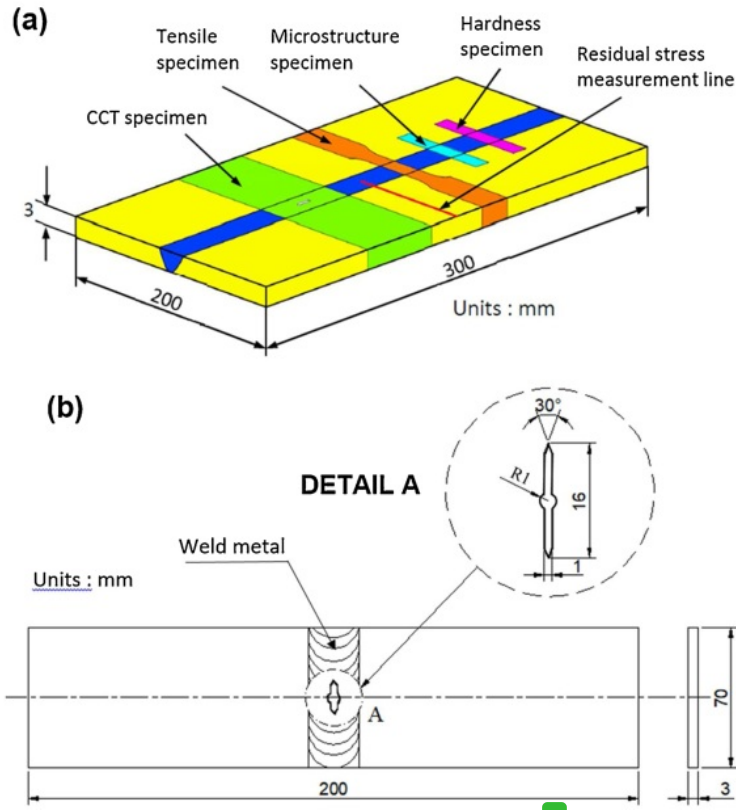
Fig. 3. (a) A schematic of welded plate showing the locations of test specimens; (b) centre-cracked tension (CCT) specimen.
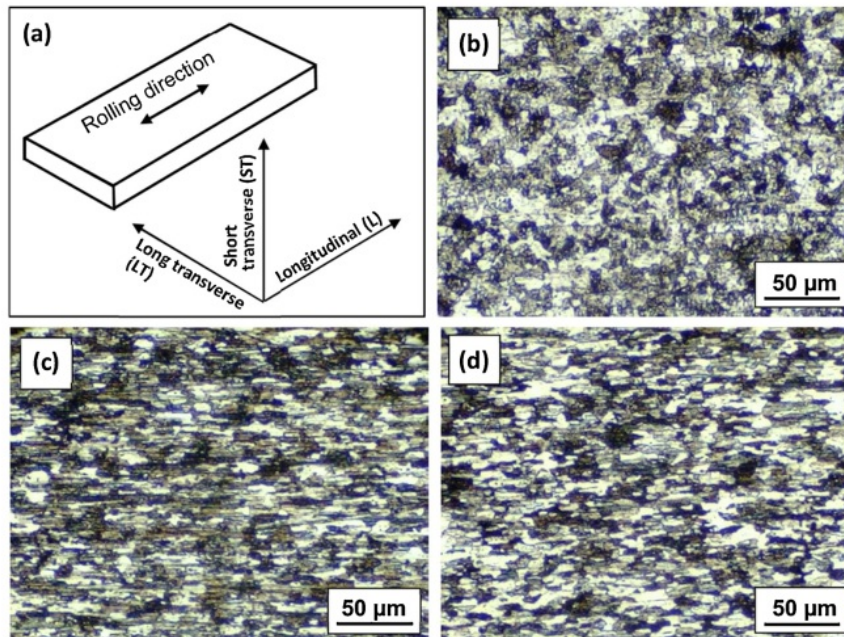

Fig. 4. (a) Three principal directions and (b),(c),(d) 5083-H116 base metal microstructures taken from longitudinal (L), short transverse (ST), long transverse (LT) respectively.

of grains to be sampled. Lattice spacings (d_i) were measured along the three principal stress directions, namely x (longitudinal), y (transverse) and z (normal) directions and the results were used to calculate residual strains (ε_i) through the following equation:

$$\varepsilon_i = \frac{d_i - d_o}{d_o} \qquad (2)$$

where d_i and d_o are lattice spacings in the strained and strain-free conditions respectively whereas subscript i represents triaxial principal directions with $i = x,y,z$. In this work, d_o was determined by measuring a small ($3 \times 3 \times 3$ mm^3) cube which was cut from one corner of the plate. However, for best accuracy, it is recommended to perform d_o measurement at every location along a measurement line using a small cube extracted from the same location. More details on d_o measurement using neutron diffraction technique can be found in Refs. [33,34]. Finally, residual stresses (σ_{ii}) were determined by substituting the strains (ε_{ii}) measured in the principal directions into Hooke's law as given by the following equation [35]:

$$\sigma_{ii} = \frac{E}{1+\nu}\varepsilon_{ii} + \frac{\nu E}{(1+\nu)(1-2\nu)}\Sigma \varepsilon_{jj} \qquad (3)$$

where E is Young's modulus and ν is Poisson's ratio.

Results and discussion

Weld thermal cycles

The analysis of weld temperature field is important in this study since it determines weld microstructure, mechanical properties and residual stress. The weld temperature field can be presented in the form of either temperature distribution or weld thermal cycle. Fig. 5 shows thermal cycles obtained from the regions at different distances of 10, 20 and 30 mm from the weld centreline. It can be seen that each thermal cycle is characterised by a steep rise of temperature during heating until a peak temperature is achieved followed by continuous cooling at a lower rate. In addition, the peak temperature and the steepness decrease with increasing distance from the weld centreline.

The peak temperature of the region at the distance of 10 mm away from the weld centreline is relatively high, i.e. 443 °C and this temperature seems to reach the α-phase field in the Al-Mg system during welding and as a consequence, this region forms HAZ after welding. Increasing distance up to 20 mm from the weld centreline leads to a sharp drop in the peak temperature to 201 °C which is below the solvus in the Al-Mg system. This temperature is not sufficient to produce HAZ and this region is referred to unaffected base metal (BM). Based on these results, the width of HAZ in the welding of 5083-H116 aluminium alloy is relatively high with the transition between HAZ and BM region occurs at a distance between 10–20 mm from the weld centreline and this will
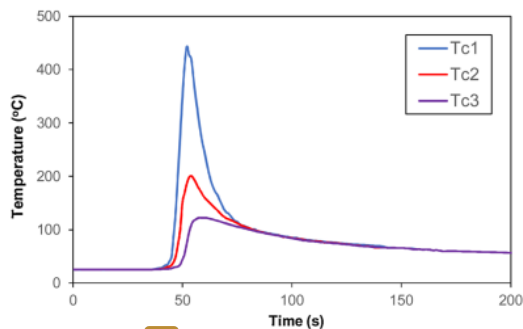

Fig. 5. Thermal cycles at the distances of 10 mm, 20 mm and 30 mm from the weld centreline.

be confirmed by the results of hardness measurements in the next section.

Microstructure analysis

Weld metal microstructures taken from the central part of the weld metals (WM) with and without vibrational treatments are shown in Fig. 6. It can be seen that weld metal microstructure in vibration-free condition (Fig. 6a) consists of equiaxed dendritic structure combined with dendritic grains. According to the classical theory of solidification, the solidification structures are controlled by G/R and cooling rate, dT/dt which is equal to GR where G is temperature gradient and R is solidification growth rate [36,37]. The former is related to constitutional supercooling ahead of solid-liquid interface which determines the growth morphology during weld solidification whereas the latter determines the grain size. The temperature gradient, G in the centre of the weld bead is relatively low so that the value of G/R is low as well and as a result, solidification structure tends to have equiaxed dendritic morphology [38].

As the mechanical vibration is applied to the weld metal at the frequency of 100 Hz as shown in Fig. 6b, considerable microstructural changes are observed. First, the percentage of equiaxed dendritic structures increases at the expense of dendritic grains and secondly, the microstructure becomes finer. It seems likely that increasing number of equiaxed dendritic grains is related to a decrease in G as a result of stirring action of vibration which allows the hot liquid to mix with the cool liquid in the weld pool hence reducing the temperature differences. On the other hand, the microstructure refinement which is associated with faster cooling rate obviously occurs in the vibrated weld despite all welding parameters are maintained constant. The plausible explanation is proposed as follow. The vibrational treatment can cause the movement of dendritic grains hence allowing the grains to come into contact with the cool liquid in the weld pool resulting in higher local cooling rate. This increasing local cooling rate leads to grain refinement [10]. Another possible explanation is that vibration can cause cavitation and under such a condition, the collapse of bubbles can cause negative pressure. Accordingly, the melting temperature is increased resulting in increased undercooling and nucleation [39,40].

The microstructural refinement continues to occur as the frequency is increased up to 300 Hz resulting in much finer microstructure as shown in Fig. 6c. However, as the frequency is increased up to 500 Hz (Fig. 6d), a reversal effect is observed with some equiaxed grains are replaced by fine columnar dendritic structures probably due to fragmentation of the equiaxed grains. In addition, another feature seen in the microstructure is the presence of dark intercellular phases, probably in the form of intermetallic compounds at interdendritic spacings. Such intermetallic compounds are also found in 5083-H321 aluminium alloy MIG weld metal under low frequency vibration [14].

Apart from the central part of the weld metals, microstructural examination was also carried out on partially melted zone (PMZ) as shown in Fig. 7. It can be seen that PMZ in as welded condition exhibits microstructure containing coarse equiaxed grains which are present along the fusion boundary. This type of microstructure is known as a non-dendritic equiaxed grain zone (EQZ). This phenomenon usually occurs in the welding of certain aluminium alloys such as 5xxx series and it has been reported that EQZ is produced through a heterogeneous nucleation of α-aluminium on intermetallic particles during weld solidification [41]. This report seems to be consistent with the microstructure in Fig. 7a in which each non-dendritic equiaxed grain of α phase is seen to have a fine intermetallic particle within the matrix α. This finding suggests that epitaxial nucleation mechanism on the HAZ substrates as commonly observed in welding of aluminium alloys no longer exists in this particular 5083-H116 alloy. In such a condition, the growth of EQZ is followed by columnar dendritic structure towards the centre part of fusion zone (FZ). Referring to Fig. 7b–d, it can be seen that under vibrational treatment, the widths of EQZ in all vibrated welds are
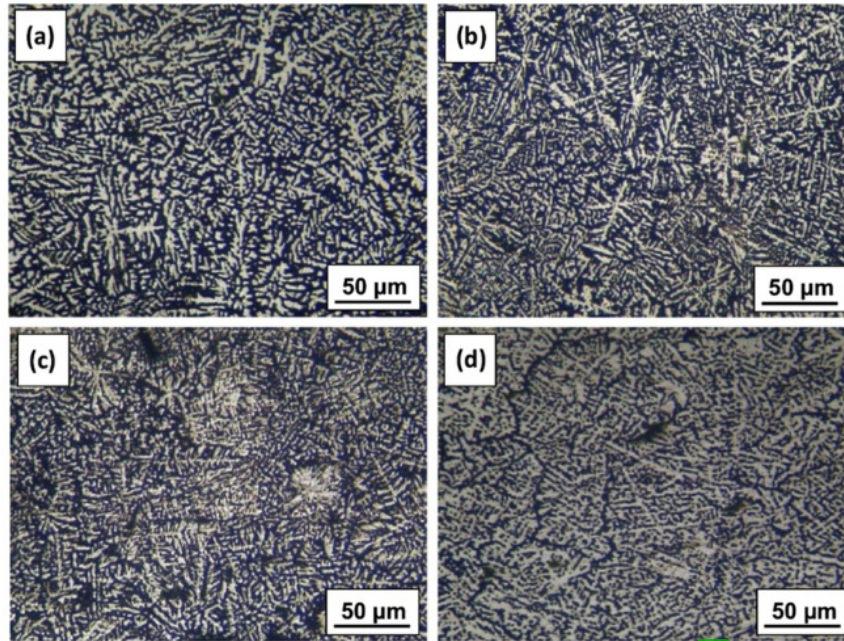
Fig. 6. Weld metal microstructures in: (a) as welded condition; (b), (c), (d) vibration treated conditions at 100 Hz, 300 Hz, 500 Hz respectively.
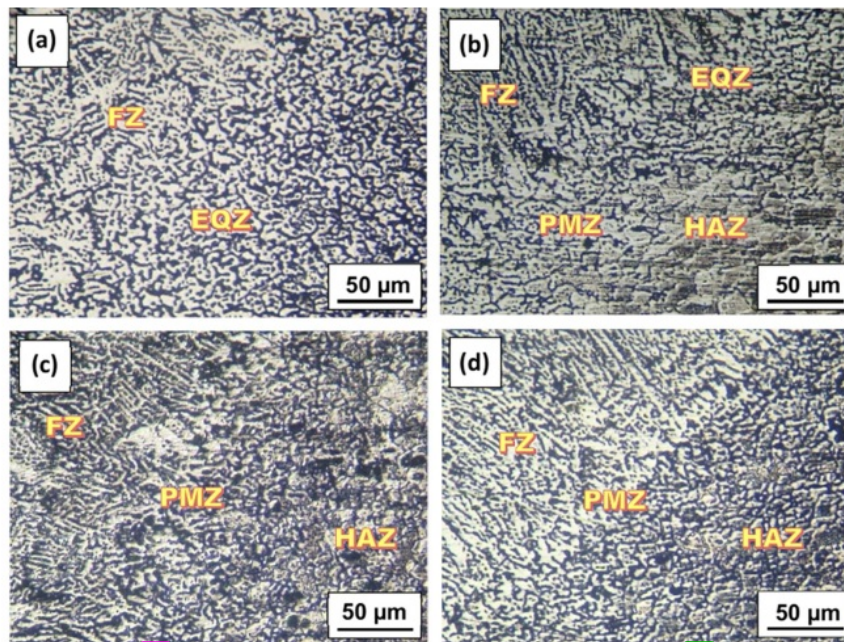

Fig. 7. Microstructures of PMZ in: (a) as welded condition; (b), (c), (d) vibration treated conditions at 100 Hz, 300 Hz, 500 Hz respectively.

reduced. It seems likely that under vibrational treatment, the intermetallic particles near the fusion line are swept by the liquid metal flow towards the central region of the weld pool hence promoting the nucleation of equiaxed dendritic structure. In addition, the width of EQZ is reduced due to reduced number of intermetallic particles near the fusion line. In such a condition, the epitaxial growth along fusion boundary is operative.

Hardness distribution

The hardness distributions of the weld joints under study are shown in Fig. 8. It can be seen that 5083-H116 aluminium alloy base metal (BM) has the average value of hardness around 110 VHN. The hardness values of heat affected zone (HAZ) in all weld joints decrease as the distance moves from the base metal towards the weld metal region and
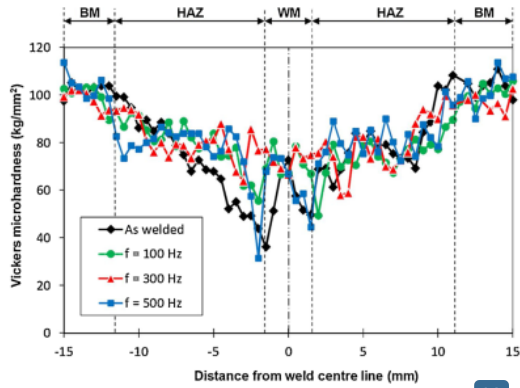
Fig. 8. Hardness profiles of the welded joints under study across weld metal (WM), heat affected zone (HAZ) and base metal (BM).

the lowest values of hardness are observed at the HAZ/weld metal (WM) boundary known as partially melted zone (PMZ). Subsequently, the hardness values increase again in the weld metal region with the peaks are present in the weld centre hence forming 'W'-shaped hardness profiles. Based on the results of microhardness measurements, the widths of HAZ for all weld joints shown in Fig. 8 are relatively large, around 8 mm, typical of welded aluminium alloys which have high thermal conductivity.

Referring to Fig. 8, it can be seen that the introduction of vibration tends to increase the hardness of weld metal and HAZ regions. According to Tian et al. [21], the higher values of hardness in weld metal region under vibrational treatment are associated with an increasing number of dislocations which lead to the formation of dislocation walls. Subsequently, these dislocation walls form low or high angle grain boundaries and as a result, the grains are refined into small grains and subgrains. Such a mechanism is referred to work hardening.

Tensile strengths

Fig. 9a shows typical engineering stress-strain curves for 5083-H116 base metal and the weld joints with and without vibration from which their average yield strength (σ_y) and ultimate tensile strength (σ_u) are obtained as shown in Fig. 9b and Table 3. The location of static fracture for all weld joints under study is observed in the weld metal region therefore, tensile properties measured in this investigation belong to weld metal region. Referring to Fig. 9a, it can be seen that the effect of vibration tends to increase the strengths of the weld metals accompanied by increased modulus of elasticity, E as indicated by increasing slopes of the linier segment in elastic region whereas the ductility values for all welds expressed as percent elongation are relatively constants around 3 %. However, the tensile properties of the welds are relatively lower compared to the 5083-H116 base metal which has yield strength, ultimate tensile strength and ductility of 230.0 MPa, 345.7 MPa and 15.6 % respectively. Further details of tensile properties of the welds can be seen in Fig. 9b and Table 3. It can be seen that as welded weld metal has yield strength and ultimate strength of 124.5 MPa and 160.5 MPa respectively. The introduction of vibration at the frequency of 100 Hz significantly increases the strengths of the weld metal and the highest strengths are observed in the weld vibrated at 300 Hz with its yield strength of 170.7 MPa and ultimate tensile strength of 242.9 MPa which are 37.1 % and 51.3 % higher than that of as welded weld metal respectively. However, as the frequency is increased to 500 Hz, the strengths of the weld tend to degrade, probably due to the presence of intermetallic compounds at interdendritic spacings as discussed previously.

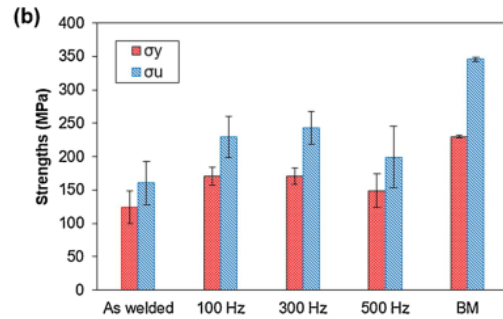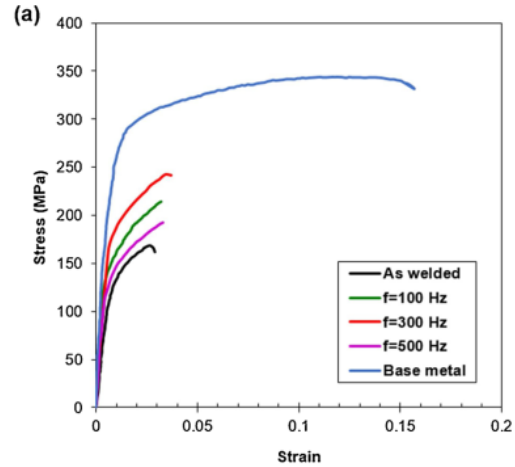The present investigation has confirmed that improved strengths of

Fig. 9. (a) Examples of stress-strain curves for the weld joints and the 5083-H116 base metal under study; (b) average yield strength, σ_y and ultimate tensile strength, σ_u obtained from the curves in (a).

Table 3
Tensile strengths of the welds.

Weld joint	Yield strength, σ_y (MPa)	Ultimate tensile strength, σ_u (MPa)
As welded	124.5 ± 24.7	160.5 ± 32.3
f = 100 Hz	170.7 ± 13.8	229.7 ± 31.0
f =300 Hz	172.5 ± 12.2	242.9 ± 24.9
f =500 Hz	148.8 ± 25.0	199.5 ± 46.0
Base metal	230.0 ± 1.9	345.7 ± 3.1

the weld joints under vibrational treatment is attributed to the formation of fine dendritic and equiaxed dendritic grains in the weld metal region according to the Hall-Petch equation [42] as follow:

$$\sigma_y = \sigma_f + \frac{k}{\sqrt{d}} \qquad (4)$$

where σ_y is the yield strength, σ_f is the friction stress against dislocation movement, k is constant which is related to the degree of dislocation accumulation behind grain boundaries and d is the average grain diameter. This finding is consistent with the previous works [16,22] which state that the improved yield and ultimate strengths of the vibration assisted weld joints are attributed to grain refinement due to mechanical vibration effect.

Residual stress

In this work, residual stress behaviour of the welds is studied by

comparing the weld vibrated at the frequency of 300 Hz and as welded weld joint as the reference. This frequency is selected because it produces excellent strength as previously discussed and good fatigue performance as will be discussed in section 3.6 and it is close to the optimum frequency reported by Hsieh et al. [43]. Fig. 10a shows longitudinal residual stress profiles for as welded weld joint and the weld vibrated at 300 Hz. In as welded condition, the tensile residual stress with the magnitude of +24.9 MPa is formed at the centre of weld metal (WM) region and it increases with increasing distance from the weld centreline until the peak of residual stress, approximately +193 MPa is achieved at fusion boundary followed by continuous drop along HAZ and the base metal hence forming M-shaped profile. Such a M-shaped residual stress profile is commonly observed in fusion welding processes. The residual stress profile of the vibrated weld joint at 300 Hz is similar to that observed in as welded weld joint in which both of them show M-shaped profiles but they are different in term of the magnitude. The introduction of vibration lowers the residual stress the weld region resulting in compressive residual stress of −107.8 MPa at the central region of the weld. Furthermore, the residual stress increases with increasing distance from the weld centreline until a peak value of +132.3 MPa is achieved in HAZ at the distance of 6 mm from the weld centreline followed by continuous decrease towards zero at the region near the plate side.

The distributions of transverse residual stress of the welds with and without vibrational treatment are shown in Fig. 10b. The central region of the weld in as welded condition is marked by the presence of compressive residual stress of −26.6 MPa. Subsequently, the residual stress increases sharply across the weld region until a maximum tensile residual stress of 125.5 MPa is achieved at fusion boundary and its adjacent HAZ region followed by slight decrease in tensile residual stress
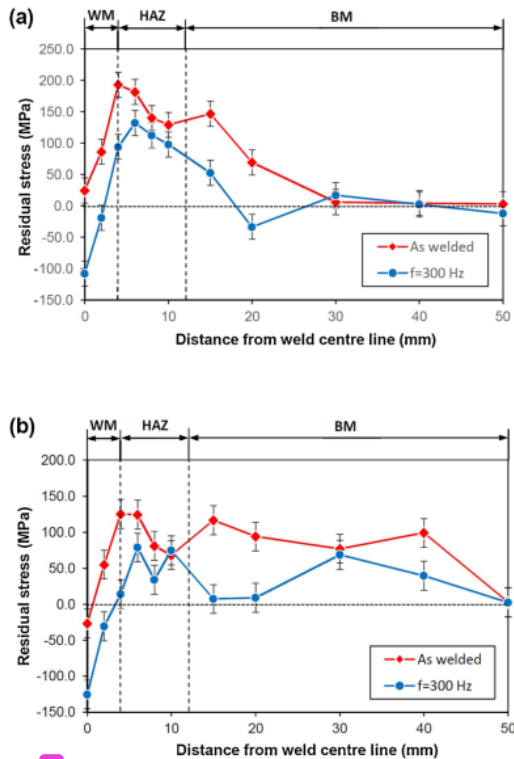
up to +75.0 MPa within HAZ region. Outside HAZ, tensile residual stress tends to be constant and it starts to decrease at the distance of 40 mm from the weld centreline. Like the results of longitudinal residual stress in Fig. 10a, the effect of vibrational treatment seems to move the transverse residual stress curve of the as welded weld joint towards negative values resulting in higher compressive residual stress in the weld centreline, typically −125.2 MPa. results of these investigation seem to confirm that the magnitudes of transverse residual stresses are relatively lower than that of longitudinal residual stresses. This is because expansion and contraction/shrinkage during welding along the transverse direction, i.e. perpendicular to weldline are lower than that in the longitudinal direction as reported previously [44]. Considering the hardness profiles in Fig. 8, it seems that compressive residual stresses in the weld region and HAZ under vibrational treatment (Fig. 10) corresponds to increasing hardness in the regions. This finding seems to suggest that the minimisation of residual stress under vibrational treatment may take place by the formation of dislocations as reported previously [21].

Fatigue crack growth rates

Fig. 11 shows fatigue crack growth behaviours of the weld metals under study presented in the plots of fatigue crack growth rate (*da/dN*) vs. stress intensity factor range (ΔK). In this work, 5083-H116 base metal was also fatigue tested as the reference. It is seen that each *da/dN*-ΔK curve in Fig. 11 starts to deviate from linearity (region II) at *da/dN* of 10^{-8} m/cycle and it asymptotically approaches a limit at a certain ΔK with decreasing *da/dN*. This condition gives an indication of the location of threshold ΔK designated as ΔK_{th}. Therefore, it may be reasonable to explain fatigue behaviours based on ΔK_{th} despite ΔK_{th} was not measured in the present investigation. Referring to Fig. 11, it can be seen that as welded weld metal exhibits the lowest ΔK_{th} among all welds under study and it has the highest fatigue crack growth rates over entire ΔK region. The introduction of vibration at the frequency of 100 Hz does not significantly change ΔK_{th} but it causes the crack growth retardation at lower ΔK, typically below 6.5 MPa $\sqrt{m}$ resulting in a plateau-like feature at the growth rate around 1.23×10^{-8} m/cycle then the crack growth rate increases again on further increase in ΔK above 6.5 MPa$\sqrt{m}$. This anomalous behaviour is often observed in a material having fine-grained microstructure which acts as grain boundary barrier for the crack to grow [45]. Subsequently, increasing the frequency at the level of 300 Hz seems to increase the ΔK_{th}. However, undesirable effect occurs on subsequent increase in the frequency up to 500 Hz with the *da/dN*-ΔK curve is shifted to the left towards as welded weld joint's curve. Another finding in this investigation is that the 5083-H116 base metal has the

Fig. 10. (a) Longitudinal residual stress; (b) transverse residual stress profiles for the welded joints in as welded condition and vibrational treatment at 300 Hz. Notes: WM is weld metal, HAZ is heat affected zone and BM is base metal.
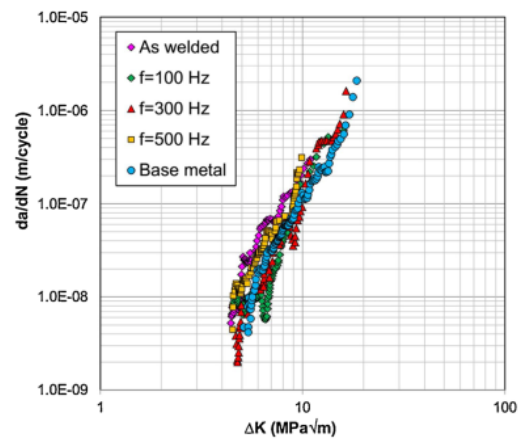

Fig. 11. Plots of *da/dN* vs. ΔK for the weld metals and 5083-H116 base metal.

highest ΔK_{th} among all welds under investigation but unlike the vibration assisted weld at 100 or 300 Hz, the 5083-H116 base metal does not show fatigue crack growth retardation in the early stage of crack growth.

The fatigue crack growth rates in region II for the weld metal under study in Fig. 11 shows linear behaviour and they can be approached by Paris law as follow:

$$da/dN = C(\Delta K)^n \tag{5}$$

where n and C are Paris constants. These Paris constants can be determined by taking a trendline in the region II for each curve and the results are shown in Fig. 12 and Table 4 where n represents the slope of the trendline and C is obtained as the line intersects the ordinate axis at $\Delta K = 1$ MPa√m.

Referring to Fig. 12 and Table 4, it can be seen that the da/dN-ΔK curve for as welded weld metal has the highest value of C, typically 9.673×10^{-11} with the n value of 3.34. The application of mechanical vibration at the frequency of 100 Hz tends to reduce the C value accompanied by a sharp increase in the slope of n around 5.76 and as a consequence, the da/dN-ΔK curve of the vibrated weld is lower than that of the weld in as welded condition at lower ΔK. However, the difference between the two curves decreases with increasing ΔK. A further increase in the frequency up to 300 Hz slightly increases da/dN with a reduced n value suggesting that at higher ΔK, typically above 9 MPa√m, the vibration assisted weld at 300 Hz has better fatigue crack growth resistance compared to the weld vibrated at 100 Hz. However, as the frequency is increased to 500 Hz, the fatigue crack growth resistance is reduced significantly with the trendline moves towards that of as welded weld metal. In comparison with all weld metals under study, the 5083-H116 base metal has moderate C and n values. The general conclusions obtained from these fatigue studies are that the improved fatigue crack growth resistances for the welds under vibrational treatment are mainly attributed to their low C values (but higher values of n) suggesting that the fatigue crack growth retardation occurs at low ΔK or at the early stage of crack growth. In such a case as this, fatigue crack growth behaviours are controlled by microstructure and residual stress. It seems that the improved fatigue crack growth resistance of the weld metals vibrated at 100 and 300 Hz is associated with the refinement of microstructure with equiaxed dendritic grains as the dominant phase. It may be argued that the lower fatigue crack growth rates in the two vibrated welds are caused by their fine grained microstructures which provide much more grain boundaries. These grain boundaries may act as barriers making the fatigue crack difficult to propagate. In addition, the equiaxed dendritic structures with their arms are oriented radially seem to produce 'interlocking structure' which may inhibit the fatigue crack
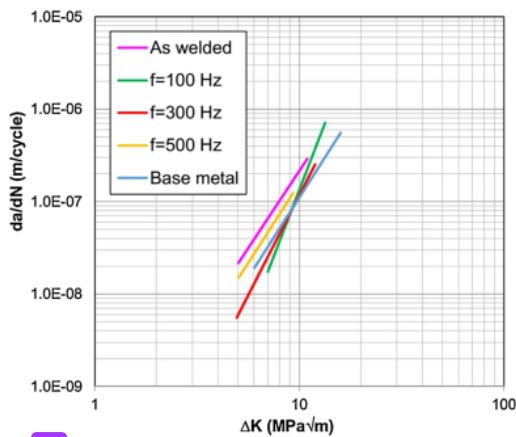

Fig. 12. Trendlines taken from stable crack growth region (region II) of da/dN vs. ΔK curves in Fig. 11.

Table 4
Paris constants of the weld metals under study.

Weld joint	C	n
As welded	9.673×10^{-11}	3.34
f = 100 Hz	2.336×10^{-13}	5.76
f = 300 Hz	5.549×10^{-12}	4.32
f = 500 Hz	5.698×10^{-11}	3.44
Base metal	3.819×10^{-11}	3.46

growth effectively. However, such a mechanism is not operative in the weld vibrated at the frequency of 500 Hz due to microstructural change with equiaxed dendritic structure is replaced by columnar dendritic structure accompanied by the occurrence of intercellular phases at interdendritic spacings as shown in Fig. 6d.

Unlike weld metal region, the 5083-H116 base metal has microstructure containing fine grains which elongate along the rolling direction, typical of wrought products as shown in Fig. 4. As commonly found in the welding of non-heat treatable 5083-H116 base metal, MIG weld joints which can be considered as cast products have lower mechanical properties compared to their base metal as shown in the results of microhardnesss and tensile tests in Figs. 8 and 9 respectively. However, from the view point of fatigue performance, the weld joint under in-process vibrational treatment at the frequency of 100 or 300 Hz could have better fatigue crack growth resistance at lower ΔK compared to its 50813-H116 base metal. This fatigue crack growth retardation could be linked to compressive residual and its mechanism is proposed as follow. Based on the previous reports [23,46–48], the presence of residual stress modify both stress ratio R and fatigue crack growth rate, da/dN as given by:

$$da/dN = C(\Delta K_{eff})^n \tag{6}$$

$$R_{eff} = \frac{K_{min} + K_{res}}{K_{max} + K_{res}} \tag{7}$$

where K_{max} and K_{min} are maximum and minimum stress intensity factors respectively whereas R_{eff} and K_{res} are stress ratio and stress intensity factor respectively which incorporate residual stress. The term of ΔK_{eff} in Eq. (6) is effective stress intensity factor range due to residual stress which is defined as:

$$\Delta K_{eff} = (K_{max} + K_{res}) - (K_{min} + K_{res}) = K_{max} - K_{min} = \Delta K \tag{8}$$

According to Eq. (8), the effect of residual stress on ΔK_{eff} seems to have disappeared with the resultant ΔK similar to that given in Eq. (5). This is because the residual stress is a mean stress effect, i.e. the residual stress changes the mean stress (σ_m) but it does not affect the stress amplitude (σ_a). This means that ΔK is not dependent on the residual stress and only the stress ratio, R is affected as given in Eq. (7). However, in the condition in which the stress ratios, R is low, the residual stress is compressive and the contribution of crack closure effect is significant as is the case for the vibrated weld in Fig. 10, then Eq. (8) is no longer valid so that corrections are required as suggested by Lados and Apelian [49] as follow:

$$\Delta K_{corr} = K_{max} + K_{res} - K_{min} = \Delta K + K_{res} \tag{9}$$

where ΔK_{corr} is the residual stress-corrected stress intensity factor range. The correction in Eq. (9) is made by adding K_{res} to K_{max} only because as the crack is fully open, there is no contact between the fatigue fracture surfaces and in such a condition, the superposition principle may apply. However, the similar correction can not be applied to K_{min} since nonlinear contact in the crack wake has occurred due to other closure mechanisms such as a roughness. Therefore, according to Eq. (9), compressive residual stress which gives negative value of K_{res} will reduce ΔK_{corr} (or ΔK_{eff} in Eq. (6)) hence lowering da/dN. In other words, the weld fatigue crack growth resistance is improved if the residual stress is compressive. Of note is that Eq. (9) is valid when the value of

K_{min} is below the stress intensity factor which corresponds to the opening, K_{op}. Such a condition is fulfilled when the residual stress is compressive and stress ratio, R is low.

To gain comprehensive understanding to fatigue crack growth mechanism of the welds under in-process vibrational treatment, SEM fractographic studies are also conducted by comparing the vibrated weld at the frequency of 300 Hz and the weld in as welded condition. This frequency is selected because it provides the best fatigue crack growth resistance. Referring to Fig. 13, it can be seen that fracture surface of as welded weld metal shows cleavage fracture with the secondary crack is observed, typical of brittle fracture. In contrast, striation like appearance is observed in the weld vibrated at the frequency of 300 Hz suggesting that this weld metal has better fatigue crack growth resistance.

Mechanisms of vibration stress relieving

Factors affecting stress relieving under vibration have been proposed by Aoki et al. [50]. According to the authors, the system of plate under transversal vibration is assumed to be a spring having a single degree of freedom, the spring is deflected by Z^e from its equilibrium position then the ratio of residual stress after vibration (σ_{sy}) to initial stress (σ_{yi}) is given by:

$$\frac{\sigma_{sy}}{\sigma_{vi}} = 0.5\left[\left(1 - \frac{Z_p^+}{Z_e}\right) + \left(1 + \frac{Z_p^-}{Z_e}\right)\right] \qquad (10)$$

where Z_p^+ and Z_p^- is permanent deformation of the spring in one direction and its opposite direction respectively. From this model, it can be seen that 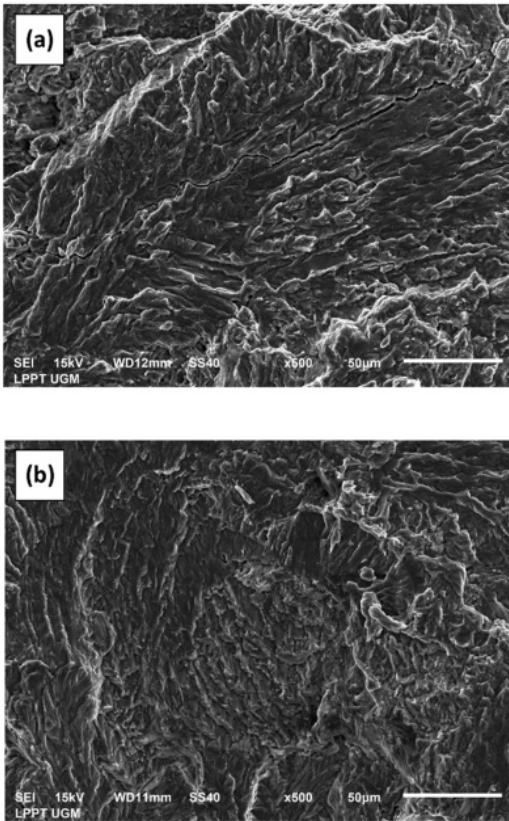deformation which in turn amplitude of excitation plays an important role in releasing residual stress with high amplitude tends to effectively release residua stress. Of note is that according to this model, the reduction of residual stress does not strongly depend on excitation frequency.

In the present study, the modification of residual stress under vibrational treatment during welding is reviewed by considering thermal stress due to expansion/contraction during welding and mechanical stress induced by vibration. The thermal stress formed immediately after welding due to longitudinal shrinkage (σ_s) as shown in Fig. 14a is given by [25]:

$$\sigma_s = \mu_l \frac{\alpha_T q_w E}{\rho c A} \qquad (11)$$

where α_T is thermal expansion coefficient, q_w is heat input, ρ is density, c is specific heat capacity, E is elastic modulus, μ_l is longitudinal stiffness factor and A is cross sectional area. On the other hand, the longitudinal stress under vibrational treatment (σ_x) for simply supported rectangular plates having the dimension of a in length, b in width and h in thickness as shown in Fig. 14b is determined by [30,51]:

$$\sigma_x = -\frac{Ez}{1-\nu^2}\left(\frac{\partial^2 w}{\partial x^2} + \nu \frac{\partial^2 w}{\partial y^2}\right) \qquad (12)$$

where w is plate deflection, ν is Poisson's ratio and z is the distance from the neutral axis to the point at which the stress is calculated. Subsequently, the plate deflection, w is determined using the following equation:

$$w(x, y, t) = \sum_{j=1}^{\infty} \sum_{k=1}^{\infty} W_{jk}(x, y) F_{jk}(t) \qquad (13)$$

$$W_{jk}(x, y) = \left(\frac{2}{\sqrt{\rho ab}}\right) \sin\frac{j\pi x}{a} \sin\frac{k\pi y}{b} \qquad (14)$$

where $F_{jk}(t)$ is a loading function for the plate loaded harmonically at one point. Referring to Eqs. (12–14), it can be seen that the plate

Fig. 13. SEM fractographs of the weld metals in: (a) as welded condition, (b) vibration treated condition at the frequency of 300 Hz.
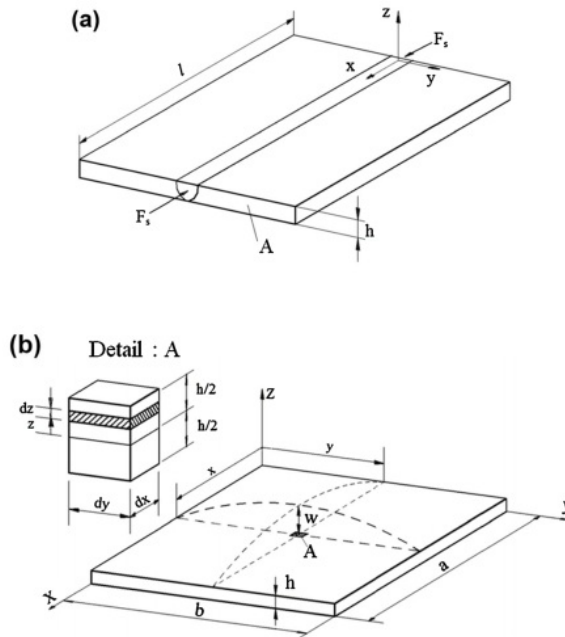

Fig. 14. (a) Longitudinal shrinkage of a welded plate with a length of l; (b) schematic of displacement-strain for a plate under vibration.

deflection which determines the longitudinal stress is dependent on the plate dimension, thermal material characteristics and excitation frequency. Subsequently, the interactions between thermal stress due to local heating during welding and mechanical stress induced by vibration could reduce residual stress resulting low tensile residual stress or even compressive residual stress in the weld region and HAZ.

The present work has shown the possible correlation between residual stress and hardness in the vibrated weld joints. It seems likely that dislocations induced by vibration play an important role in the modification of residual stress. Therefore, further studies on dislocations needs to be conducted.

Conclusions

The present work has experimentally investigated strength and fatigue crack growth properties of metal inert gas (MIG) 5083-H116 aluminum alloy welded joints under in-process vibrational treatment and the following conclusions are drawn from this study.

(1) The application of vibration at low frequencies, typically in the range of 100–500 Hz to MIG welding of AA5083-H116 aluminium alloy causes two microstructural changes, i.e. grain refinement accompanied by an increase in the amount of equiaxed structure in the central region of the weld metal at the expense of dendritic microstructure.

(2) Higher strengths are observed in the vibration assist welded joints, especially at the frequency of 300 Hz with the increase in yield strength and ultimate tensile strength up to 37.1 and 51.3 % respectively in comparison with the weld in as welded condition. These strength improvements are related to fine grained microstructure in the vibrated welds according to Hall-Petch relationship. However, the strengths are degraded as the weld metal microstructure contains intermetallic compounds which are precipitated at interdendritic spacings at higher frequency, typically 500 Hz.

(3) The hardness in the weld region and HAZ of the weld joints under in-process vibrational treatment tends to increase. This increasing hardness is associated with compressive residual stress in both regions.

(4) The grain refinement and reduced residual stress resulted from in-process vibrational treatment are likely to be the main factors improving weld fatigue crack growth resistance. However, more works would be required in the future to clarify this finding.

Declaration of Competing Interest

Acknowledgments

References

[1] Jose MJ, Kumar SS, Sharma A. Vibration assisted welding processes and their influence on quality of welds during solidification. Sci Technol Weld Join 2015;21(4):243–58.

[2] Song J, Zhang Y. Eff ;ect of vibratory stress relief on fatigue life of aluminum alloy 7075–T651. Adv Mech Eng 2016;8:1–9.

[3] Shah U, Liu X. Effects of ultrasonic vibration on resistance spot welding of transformation induced plasticity steel 780 to aluminum alloy AA6061. Mater Des 2019;182:108053.

[4] Cui Y, Xu CL, Han Q. Effect of ultrasonic vibration on unmixed zone formation. Scripta Mater 2006;55:975–8.

[5] Radel T. Mechanical manipulation of solidification during laser beam welding of aluminium. Weld World 2018;62:29–38.

[6] Reddy GM, Gokhale AA, Rao KP. Weld microstructure refinement in a 1441 grade aluminium-lithium alloy. J Mater Sci 1997;32:4117–26.

[7] Krajewski A, Wlosinski W, Chmielewski T, Kolodziejczak P. Ultrasonic-vibration assisted arc-welding of aluminum alloys. Bull Pol Ac:Tech 2012;60(4):841–52.

[8] Yuan T, Kou S, Luo Z. Grain refining by ultrasonic stirring of the weld pool. Acta Mater 2016;106:144–54.

[9] Liu X, Osawa Y, Takamori S, Mukai T. Grain refinement of AZ91 alloy by introducing ultrasonic vibration during solidification. Mater Lett 2008;62:2872–5.

[10] Kuo CW, Yang SM, Chen JH, Lai GH, Wu W. Study of vibration welding mechanism. Sci Technol Weld Join 2008;13(4):357–62.

[11] Sabzi M, Dezfuli SM. Drastic improvement in mechanical properties and weldability of 316L stainless steel weld joints by using electromagnetic vibration during GTAW process. J Manuf Process 2018;33:74–85.

[12] Campbell J. Effects of vibration during solidification. Int Met Rev 1981;2:71–108.

[13] Tewari SP. Effects of oscillation on impact property of weldments. ISIJ Int 1999;39(8):809–12.

[14] Tamasgavabari R, Ebrahimi AR, Abbasi SM, Yazdipour AR. The effect of harmonic vibration with a frequency below the resonant range on the mechanical properties of AA-5083-H321 aluminum alloy GMAW welded parts. Mater Sci Eng A 2018;736:248–57.

[15] Zhong Y, Wang H, Wang Y, Wang J, Shen Z, Ren Z, et al. Effects of electromagnetic vibration frequencies on microstructure and tensile properties of Al-15 wt pct Sn Alloy in semi-continuous casting process. Metal Mater Trans A 2017;48A:3377–88.

[16] Watanabe T, Shiroki M, Yanagisawa A, Sasaki T. Improvement of mechanical properties of ferritic stainless steel weld metal by ultrasonic vibration. J Mater Process Technol 2010;210:1646–51.

[17] Qingmei L, Yong Z, Yaoling S, Feipeng Q, Qijie Z. Influence of ultrasonic vibration on mechanical properties and microstructure of 1Cr18Ni9Ti stainless steel. Mater Des 2007;28:1949–52.

[18] Pucko B, Gliha V. Charpy toughness and microstructure of vibrated weld metal. Sci Technol Weld Join 2006;11(3):289–94.

[19] Tewari SP, Shanker A. Effects of longitudinal vibration on hardness of the weldments. ISIJ Int 1993;33(12):1265–9.

[20] Tarasov SY, Vorontsov AV, Fortuna SV, Rubtsov VE, Krasnoveikin VA, Kolubaev EA. Ultrasonic-assisted laser welding on AISI 321 stainless steel. Weld World 2019;63:875–86.

[21] Tian Y, Shen J, Hu S, Wang Z, Gou J. Effects of ultrasonic vibration in the CMT process on welded joints of Al alloy. J Mater Process Technol 2018;259:282–91.

[22] Wu W. Influence of vibration frequency on solidification of weldments. Scripta Mater 2000;42:661–5.

[23] Pan L, Athreya BP, Forck JA, Huang W, Zhang L, Hong T, et al. Welding residual stress impact on fatigue life of a welded structure. Weld World 2013;57:685–91.

[24] Gao H, Zhang Y, Wu Q, Song J, Wen K. Fatigue life of 7075-T651 aluminium alloy treated with vibratory stress. Int J Fatigue 2018;108:62–7.

[25] Radaj D. Heat Effects of Welding: temperature field, residual stress, distortion. Berlin: Springer-Verlag; 1992.

[26] Rozumek D, Lewandowski J, Lesiuk G, Correia. The influence of heat treatment on the behavior of fatigue crack growth in welded joints made of S355 under bending loading. Int J Fatigue 2020;131:105328.

[27] da Silva ALL, Correia JAFO, de Jesus AMP, Lesiuk G, Fernandes AA, Calcada R, et al. Influence of fillet end geometry on fatigue behaviour of welded joints. Int J Fatigue 2019;123:196–212.

[28] Wu M, Wu CS, Gao S. Effect of ultrasonic vibration on fatigue performance of AA2024-T3 friction stir weld joints. J Manuf Process 2017;29:85–95.

[29] Liang X, Wan Y, Zhang C, Zhang B, Meng X. Comprehensive evaluation of welding quality for butt-welded by means of CO_2 arc vibratory welding. Int J Adv Manuf Technol 2017;90:1911–20.

[30] Benaroya H. Mechanical vibration. New Jersey: Prentice-Hall; 1998.

[31] ASTM. E8/E8M-16. Standard test methods for tension testing of metallic materials. West Conshohocken, PA: ASTM International; 2016.

[32] ASTM. E647-00. Standard test method for measurement of fatigue crack growth rates. Annual book of ASTM standards, Vol. 03.01. ASTM International; 2000.

[33] Jacob A, Mehmanparast A, D'Urzo R, Kelleher J. Experimental and numerical investigation of residual stress effects on fatigue crack growth behaviour of S355 steel weldments. Int J Fatigue 2019;128:105196.

[34] Jacob A, Oliveira J, Mehmanparast A, Hosseinzadeh F, Kelleher J, Berto F. Residual stress measurements in offshore wind monopile weldments using neutron diffraction technique and contour method. Theor Appl Fract Mech 2018;96:418–27.

[35] Pratihar S, Turski M, Edwards L, Bouchard PJ. Neutron diffraction residual stress measurements in a 316L stainless steel bead-on-plate weld specimen. Int J Press Vess Piping 2009;86:13–9.

[36] Kou S. Welding metallurgy. 2nd ed. New Jersey: John Willey & Sons, Inc; 2003.

[37] David SA, Vitek JM. Correlation between solidification parameters and weld microstructures. Int Met Rev 1989;34(5):213–45.

[38] Schempp P, Rethmeier M. Understanding grain refinement in aluminium welding. Weld World 2015;59:767–84.

[39] Wang G, Dargusch MS, Qian M, Eskin DG, St John DH. The role of ultrasonic treatment in refining the as-cast grain structure during the solidification of an Al-2Cu alloy. J Cryst Growth 2014;408:119–24.

[40] Borkent BM, Gekle S, Prosperetti A, Lohse D. Nucleation threshold and deactivation mechanisms of nanoscopic cavitation nuclei. Phys Fluids 2009;21(10):1065–73.

[41] Kostrivas A, Lippold JC. Fusion boundary microstructure evolution in aluminium alloys. Weld World 2006;60(11/12):24–34.

[42] Reed-Hill RE, Abbaschian R. Physical metallurgy principles. 3rd ed. Boston: PWS Publishing Company; 1994.

[43] Hsieh CC, Lai CH, Wu W. Effect of vibration on microstructures and mechanical properties of 304 stainless steel GTA welds. Met Mater Int 2013;19(4):835–44.

[44] Ilman MN, Triwibowo NA, Wahyudianto A, Muslih MR. Environmentally assisted fatigue behaviour of stress relieved metal inert gas (MIG) AA5083 welds in 3.5% NaCl solution. Int J Fatigue 2017;100:285–95.

[45] Richard HA, Sander M. Fatigue crack growth. Springer International Publishing; 2016.

[46] Ilman MN, Kusmono Muslih MR, Subeki N, Wibowo H. Mitigating distortion and residual stress by static thermal tensioning to improve fatigue crack growth performance of MIG AA5083 welds. Mater Des 2016;99:273–83.

[47] Ma YE, Staron P, Fischer T, Irving PE. Size effects on residual stress and fatigue crack growth in friction stir welded 2195-T8 aluminium-Part II: modelling. Int J Fatigue 2011;33:1426–34.

[48] Lammi CJ, Lados DA. Effects of processing residual stresses on fatigue crack growth behaviour of structural materials: experimental approaches and microstructural mechanisms. Metall Mater Trans A 2012;43A:87–107.

[49] Lados DA, Apelian D. The effect of residual stress on the fatigue crack growth behavior of Al-Si-Mg cast alloys-Mechanisms and corrective mathematical models. Metall Mater Trans A 2006;37A:133–45.

[50] Aoki S, Nishimura T, Hiroi T, Hirai S. Reduction method for residual stress of welded joint using harmonic vibrational load. Nucl Eng Des 2007;237:206–12.

[51] Szilard R. Theory and analysis of plates: classical and numerical methods. New York: Prentice-Hall, Inc.; 1973.

1-s2.0-S1526612520307039-main_Jurnal_Bowo_Q1.pdf

18% SIMILARITY INDEX

6% INTERNET SOURCES

17% PUBLICATIONS

2% STUDENT PAPERS

PRIMARY SOURCES

1. M.N. Ilman, Kusmono, M.R. Muslih, N. Subeki, H. Wibowo. "Mitigating distortion and residual stress by static thermal tensioning to improve fatigue crack growth performance of MIG AA5083 welds", Materials & Design, 2016
Publication — 4%

2. M.N. Ilman, N.A. Triwibowo, A. Wahyudianto, M.R. Muslih. "Environmentally assisted fatigue behaviour of stress relieved metal inert gas (MIG) AA5083 welds in 3.5% NaCl solution", International Journal of Fatigue, 2017
Publication — 3%

3. eprints.gla.ac.uk
Internet Source — 1%

4. worldwidescience.org
Internet Source — 1%

5. M.N. Ilman. "Chromate inhibition of environmentally assisted fatigue crack propagation of aluminium alloy AA 2024-T3 in 3.5% NaCl solution", International Journal of — 1%

Fatigue, 2014
Publication

6   D LADOS, D APELIAN, J DONALD. "Fracture mechanics analysis for residual stress and crack closure corrections", International Journal of Fatigue, 2007
Publication

1%

7   Submitted to Universitas Muhammadiyah Surakarta
Student Paper

1%

8   Shigeru Aoki, Tadashi Nishimura, Tetsumaro Hiroi, Seiji Hirai. "Reduction method for residual stress of welded joint using harmonic vibrational load", Nuclear Engineering and Design, 2007
Publication

<1%

9   www.science.gov
Internet Source

<1%

10 Masoud Sabzi, Saeid Mersagh Dezfuli. "Drastic improvement in mechanical properties and weldability of 316L stainless steel weld joints by using electromagnetic vibration during GTAW process", Journal of Manufacturing Processes, 2018
Publication

<1%

11 S. Pratihar, M. Turski, L. Edwards, P.J. Bouchard. "Neutron diffraction residual stress measurements in a 316L stainless steel bead-

<1%

on-plate weld specimen", International Journal of Pressure Vessels and Piping, 2009
Publication

12 P. SIVARAJ, D. KANAGARAJAN, V. BALASUBRAMANIAN. "Fatigue crack growth behaviour of friction stir welded AA7075-T651 aluminium alloy joints", Transactions of Nonferrous Metals Society of China, 2014
Publication
<1%

13 www.mdpi.com
Internet Source
<1%

14 Ilman, M.N., Kusmono, M.R. Muslih, N. Subeki, and H. Wibowo. "Mitigating distortion and residual stress by static thermal tensioning to improve fatigue crack growth performance of MIG AA5083 welds", Materials & Design, 2016.
Publication
<1%

15 Solid Mechanics and Its Applications, 2008.
Publication
<1%

16 iom3.tandfonline.com
Internet Source
<1%

17 "Light Metals 2020", Springer Science and Business Media LLC, 2020
Publication
<1%

18 Takehiko Watanabe, Masataka Shiroki, Atsushi Yanagisawa, Tomohiro Sasaki. "Improvement of
<1%

mechanical properties of ferritic stainless steel weld metal by ultrasonic vibration", Journal of Materials Processing Technology, 2010
Publication

19   link.springer.com
      Internet Source   <1%

20   Diana A. Lados, Diran Apelian. "The effect of residual stress on the fatigue crack growth behavior of Al-Si-Mg cast alloys—Mechanisms and corrective mathematical models", Metallurgical and Materials Transactions A, 2006
      Publication   <1%

21   www.scribd.com
      Internet Source   <1%

22   I. TAKAHASHI. "Automatic restraint and visual detection of fatigue crack growth by applying an alumina paste", Fatigue & Fracture of Engineering Materials and Structures, 8/2007
      Publication   <1%

23   www.ir.nctu.edu.tw
      Internet Source   <1%

24   Submitted to Universitas Sebelas Maret
      Student Paper   <1%

25   Dariusz Rozumek, Janusz Lewandowski, Grzegorz Lesiuk, José A. Correia. "The
                                                                         <1%

influence of heat treatment on the behavior of fatigue crack growth in welded joints made of S355 under bending loading", International Journal of Fatigue, 2020
Publication

26 www.tandfonline.com
    Internet Source   <1%

27 Submitted to Chulalongkorn University
    Student Paper   <1%

28 X. CHEN, K. AN, K. S. KIM. "Low-cycle fatigue of 1Cr–18Ni–9Ti stainless steel and related weld metal under axial, torsional and 90° out-of-phase loading", Fatigue & Fracture of Engineering Materials & Structures, 2004
    Publication   <1%

29 Pengfei Gao, Tie Liu, Chao Wang, Anping Wu, Zhanliang Li, Guojian Li, Qiang Wang. "Frequency dependence of sound field effect on microstructure and wear performance of plasma sprayed Ni-10 wt.%Al coatings", Surface and Coatings Technology, 2020
    Publication   <1%

30 Sharma, Sunil, and Krishnamoorthy Balachandar. "Comparative Study of Constant Current and Pulsed Current GTA-Welded Al-B_4C Stir Cast Composite", Applied Mechanics and Materials, 2015.
                                                                       <1%

Publication

31 Review of Progress in Quantitative Nondestructive Evaluation, 1983.
Publication
<1%

32 Submitted to Kennedy-Western University
Student Paper
<1%

33 orbi.uliege.be
Internet Source
<1%

34 iopscience.iop.org
Internet Source
<1%

35 Submitted to University of Birmingham
Student Paper
<1%

36 Shanmugam, K.. "Effect of weld metal properties on fatigue crack growth behaviour of gas tungsten arc welded AISI 409M grade ferritic stainless steel joints", International Journal of Pressure Vessels and Piping, 200908
Publication
<1%

37 "Proceedings of the 9th International Symposium on Superalloy 718 & Derivatives: Energy, Aerospace, and Industrial Applications", Springer Science and Business Media LLC, 2018
Publication
<1%

38 A.K. Lakshminarayanan, V. Balasubramanian, G. Madhusudhan Reddy. "On the fatigue
<1%

behaviour of electron beam and gas tungsten arc weldments of 409M grade ferritic stainless steel", Materials & Design, 2012
Publication

39   Weifeng Xie, Chunli Yang. "Microstructure, mechanical properties and corrosion behavior of austenitic stainless steel sheet joints welded by gas tungsten arc (GTA) and ultrasonic–wave–assisted gas tungsten pulsed arc (U–GTPA)", Archives of Civil and Mechanical Engineering, 2020
Publication

<1%

40   Noritake Oguchi, Junichi Sakai, Hiroyuki Inoue, Shigeru Komukai. "Critical Hardness for HSC in Deposit Welding on Steel Line Pipes Under Cathodic Protection", Volume 2: Integrity Management; Poster Session; Student Paper Competition, 2006
Publication

<1%

41   M. N. JAMES, D. J. HUGHES, D. G. HATTINGH, G. R. BRADLEY, G. MILLS, P. J. WEBSTER. "Synchrotron diffraction measurement of residual stresses in friction stir welded 5383-H321 aluminium butt joints and their modification by fatigue cycling", Fatigue & Fracture of Engineering Materials & Structures, 2004
Publication

<1%

| Exclude quotes | On | Exclude matches | < 10 words |
| Exclude bibliography | On | | |